Fan Performance Analysis for Rotor Cooling of Axial Flux Permanent Magnet Machines

Fawzal, AS, Cirstea, RM, Gyftakis, KN, Woolmer, TJ, Dickison, M & Blundell, M

Original citation & hyperlink:
Fawzal, AS, Cirstea, RM, Gyftakis, KN, Woolmer, TJ, Dickison, M & Blundell, M 2017, 'Fan Performance Analysis for Rotor Cooling of Axial Flux Permanent Magnet Machines' *IEEE Transactions on Industry Applications*, vol 54, no. 4, pp. 3295-3304
https://dx.doi.org/10.1109/TIA.2017.2675986

DOI 10.1109/TIA.2017.2675986
ISSN 0093-9994
ESSN 1939-9367

Publisher: IEEE

Fan Performance Analysis for Rotor Cooling of Axial Flux Permanent Magnet Machines

A. S. Fawzal, R. M. Cirstea, K. N. Gyftakis, T. J. Woolmer, M. Dickison and M. Blundell

***Abstract* – The thermal management of an Axial Flux Permanent Magnet (AFPM) machine is essential because it determines the machine's continuous power output and reliability. In this paper, a secondary cooling method is proposed using rotor cooling which allows better thermal management on the permanent magnets that are attached to the rotor. This will reduce the potential of the machine failing due to magnet demagnetization and degradation. Thermal analysis via Lumped Parameter (LM) networks is usually sufficient in predicting the motor's thermal behaviour. However, the accuracy of the prediction can be increased especially for devices with complex flow regions by Computational Fluid Dynamics (CFD). In this study, the fan blade was attached to the rotor of a Yokeless and Segmented Armature (YASA) machine for flow validation and then three different fan blade designs from other engineering applications were tested. The evaluation includes the flow characteristic, power requirement and thermal characteristic for the AFPM's rotor cooling applications. Additionally, the Rotor Cooling Performance Index (RCPI) is introduced to assess each fan design performance.**

***Index Terms*—Axial flux, Permanent magnet machines, Fluid dynamics, Rotors, Cooling, Fluid flow, Thermal analysis, CFD, SAT, Yokeless and segmented armature machine.**

I. INTRODUCTION

BASED on legislation constraints, the Directive 2009/28/EC of 23 April 2009 [1] and the Commission Regulation 640/2009/EC of 22 July 2009 [2], a new development of electric machine topology with better efficiency and high power density is needed in relation to the eco-design guideline. To meet this requirement, an Axial Flux Permanent Magnet (AFPM) machine is well suited for transport and traction applications. This is due to its high power, high torque density and short axial length [3]–[5]. The advancement of AFPM topology was continued by the Segmented Armature Torus (SAT) topology; also known as the Yokeless and Segmented Armature (YASA) which improved the torque density and efficiency over conventional AFPM machines. Derived from dual-rotor single-stator AFPM torus topology, the YASA machine combines NS and NN Torus-S topologies [6], resulting in an AFPM that is lightweight and compact in its class.

AFPM machines are categorised as disc type electrical machines because the rotor is present in a form of disc and the flux path is travel axially. This makes the machine package compact because the stator and rotor arrangements are side-by-side. Even with less complex design topology, the internal temperature needs to be predicted during the design stage in order to avoid overheating. In general, energy conversion from electricity to mechanical motion produces losses that are manifested as heat. The operating temperature of an electrical machine can be controlled by balancing between the heat generated and the heat removal rate. Controlling the machine's operating temperature is crucial, as this will determine its continuous power output, machine reliability and also to avoid any catastrophic failure caused by degradation [8]–[10]. By doing so, the maximum potential of a machine can be achieved, the life-span of the machine can be prolonged and operating life can be optimised. As described by Fitzgerald et al., the deterioration is a function of time and temperature [7]. Therefore, understanding the heat generation and cooling method is required to avoid deterioration and thus create a reliable machine.

Extensive research on the electromagnetic analysis of AFPM machines has been undertaken, yet limited research using Computational Fluid Dynamics (CFD) on the thermal aspect has been carried out [11], particularly compared to radial flux permanent magnet counterparts. Conventionally, Lumped Parameter (LM) networks of one-dimensional [12], and two-dimensional [13] approaches have been used in predicting the thermal behaviour of AFPM by compiling both solid and fluid domains. This method is favourable to AFPM machine designers because it gives a fast solution over a broad range of machine speeds. However, LP method does not include any fluid domain changes related to design variation (e.g. inlet/outlet, rotor, magnet arrangement, etc.). Therefore, CFD modelling is required to understand the complexity of the flow and the thermal behaviour at the expense of higher computational cost [14]. Furthermore, CFD can also be used to increase the accuracy of a LP thermal model by providing the windage losses and the heat transfer coefficients as a function of speed for the rotating component in the system

This work was funded and supported by Coventry University and YASA Motor Ltd., United Kingdom.

A. S. Fawzal is with the Faculty of Engineering, Environment & Computing, Coventry University, Priory Street, Coventry, CV1 5FB, UK (email: fawzala@uni.coventry.ac.uk).

R. M. Cirstea is with the School of Mechanical, Aerospace and Automotive Engineering, Coventry University, Priory Street, Coventry, CV1 5FB, UK (email: aa9340@coventry.ac.uk).

K. N. Gyftakis is with School of CEM and the Centre for Mobility and Transport, Coventry University, Priory Street, Coventry, CV1 5FB, UK (email: k.n.gyftakis@ieee.org).

T. J. Woolmer is with YASA Motors Ltd. Abingdon, Oxfordshire, OX14 4SD, UK (email: tim.woolmer@yasamotors.com)

M. Dickison is with the Faculty of Engineering, Environment & Computing, Coventry University, Priory Street, Coventry, CV1 5FB, UK (email: aa7111@coventry.ac.uk).

M. Blundell is with the Centre for Mobility and Transport, Coventry University, Priory Street, Coventry, CV1 5FB, UK (email: cex403@coventry.ac.uk).

[15][16].

This paper presents CFD analysis of different rotor fan blade designs for rotor cooling on AFPM machines specifically considering YASA machine topology. This secondary cooling method is unique compared to conventional rotor cooling because the fan blade is attached directly to the machine rotor; hence the rotor provides the air flow and dissipates the heat at the same time. The focus of this study was to evaluate the fan performance including power requirements to spin the rotor (also known as windage losses). CFD flow validation was conducted at the initial stage before the evaluation begins. Additionally, static temperature was added, to provide insight on the heat convection of each fan blade design. The initial work has being presented in [17].

II. The Yokeless and Segmented Armature (YASA) Machine and Its Cooling Mechanism

Conventional AFPM machines are comprised of yokes on the rotor and stator to support its field system and protect the armature of the motor. The YASA machine topology is able to improve the performance of AFPM by removing the stator yoke and implementing other design changes, as illustrated in Fig. 1. The derivation of the YASA topology began with the NS Torus-S topology (Fig. 1-a), then evolved by excluding the stator yoke as it did not seriously impact the electromagnetic behaviour of the system (Fig. 1-b). In Fig. 1-c, the YASA topology was formed by the pitch of the teeth is enlarged and square windings are used. This new topology improved torque density by 20% and recorded a peak efficiency of 95% with 50% less iron in the stator compared to a conventional AFPM machine [6]. Nevertheless, the full potential of the machine is currently limited by its operating temperature. Therefore, optimisation of the thermal design is required to improve the motor's reliability and to further increase its performance.

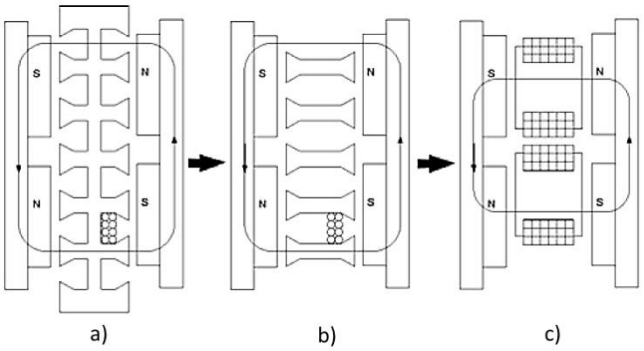

Fig. 1. YASA derivation topology begins with (a) NS Torus-S topology, (b) exclude the stator yoke and (c) final design changes [6].

The current YASA machine design uses oil as a direct stator cooling method to counter the heat generated from iron and copper losses. This is accomplished by sealing the stator assembly from the rotors and allows coolant oil to pass through between the windings. Camilleri et al. [18] have investigated this cooling method and mapped the temperature profile of the YASA machine pole piece for different coolant flow rates. The study on this machine also considered the influence of stator coolant flow path geometry [19]. The findings provided sufficient thermal management for low and medium continuous power applications.

To boost up the performance of this machine even further, a secondary cooling method has been introduced by using a rotor cooling technique. This is to allow additional thermal management on eddy currents and stray losses of the magnets and the rotor.

III. AFPM Rotor Cooling and Fan Blade Design

The initial concept of rotor cooling for the AFPM machine was first proposed by Vansompel [4]. The implementation of rotor cooling on the current YASA machine topology was accomplished by introducing an opening at the centre of the rotor and a single outlet on the radial cover. This is adopted from the concept of a centrifugal fan, where the air will flow from the centre inlet through the system that drives by a fan blade and exits through the side outlet. Fig. 2 shows that the fan blade component is attached directly to the machine rotor of non drive end side. While the machine rotates, the rotor with a fan blade will create pressure gradient inside the system, thus air flow is developed. This air flow is expected to absorb the heat from the rotor (by convection) and disperse it to the outlet. As this happens, heat from the magnet will flow to the rotor assembly through conductive heat transfer.

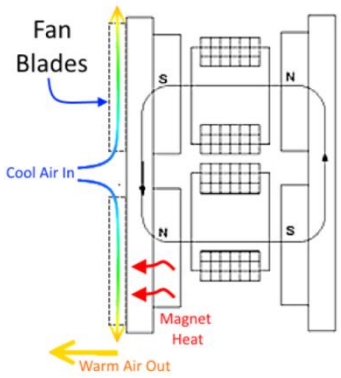

Fig. 2. The position of fan blade attached to the rotor allows introduction of cool air in the system.

The rotor cooling approach has not only increased the machine reliability but also the YASA machine's continuous power by 43% and the torque by 20% [20][21]. This is because, the temperature on the magnets becomes lower and more loads can be amplified until the magnets reach its maximum allowable temperature. The current performance values in [20][21] were achieved by using backward-inclined aerofoil blade because the fan blade design meet specific mass flow rate and pressure requirements. However, there is limited understanding on its contribution towards heat transfer aspects.

For this purpose, three different fan blade designs were selected from other engineering applications in order to assess the flow characteristic, power requirement (windage losses) and thermal characteristic. Fig. 3 shows the selection of fan blade designs, which are: Fig. 3-a, a backward-inclined aerofoil blade – from a force-draft blower application [22],

Fig. 3-b, a radial aerofoil blade – from a typical fan engineering application [22] and Fig. 3-c, a tear drop pillar blade – from an automotive disc brake [23]. The backward-inclined aerofoil blade and radial aerofoil blade were selected as it is known that they provide good air flow as a pump or fan. Additionally, it is interesting to see how a tear drop pillar blade performs as this is the cooling technique used for heat removal in brake disc.

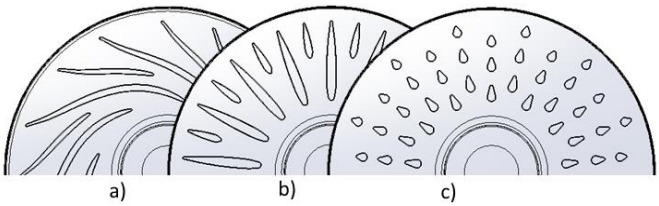

Fig. 3. The fan blade design selection with (a) backward-inclined aerofoil blade [20], (b) radial aerofoil blade [20] and (c) tear drop pillar blade [21].

For rotor cooling applications, the operation of a backward-inclined aerofoil blade is limited to an unidirectional machine, while the radial aerofoil blade and the tear drop pillar blade can be used in a machine with a bi-directional application. In this study, unidirectional operational was considered because current machine design is specific for automotive traction application with medium rotational speed in the intended directionand slow speed in the reverse.

IV. Experimental Rig

The flow measurement was carried out on a 160kW YASA machine that is in production by YASA Motors Ltd. The dimensions of the rotor inner and outer diameter are 77.0mm and 252.7mm respectively. The clearences in the system by gap ratio, *s/R* are: magnet-to-stator 0.00396, rotor-to-stator 0.02453 and rotor-to-cover 0.00594, where *s* is the gap distance and *R* is the outer diameter. There was a trigger disc mounted on the rotor vanes axial surface to measure the rotational speed of the rotor and this disc also acted as a seal to avoid air spillage during operation.

For validation purposes, this machine was set to run without a load in order to assess the mass flow rate generated by the backward-inclined aerofoil blade that was attached to the disc rotor. The machine was equipped with a dual PMF4104V mass flow sensor at the inlet opening of the machine cover, as shown in Fig. 4. These mass flow sensors are equiped with temperature compensation for accuracy which allows independence from the inlet air temperature gradient.

The mass flow rate was recorded from 1000rpm to 3500rpm for every 500rpm of rotational speed. This is equivalent to a rotational Reynolds number (*Re*) of 1.07e5 to 3.73e5 at the outer edge of the rotor disk. This speed range was selected based on the limitation of the mass flow sensor (limited to 600litres/min), while the nominal speed of the machine is 2100rpm. The speed was held until the system reached a steady state condition for mass flow rate measurement and in between of 100rpm test points, the speed was ramped at 10rpm/s.

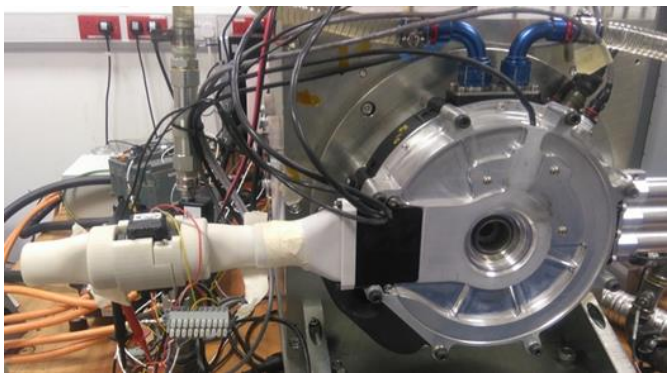
Fig. 4. The experimental rig with mass flow sensor at the inlet.

V. CFD Model

The complex 3D CAD design was simplified by removing features that are irrelevant to fluid flow and known to have limited or zero contribution to the flow and thermal aspects. The major CAD simplification was done using SolidWorks 2014 and the fluid volume was extracted. The 3D model was then imported into STAR-CCM+ v9.04 for further design simplification and merging the solid parts as a single solid domain. This includes the magnets circular array, the rotor fan blade and the trigger disc. In addition, the fluid domain was split into two parts to differentiate between static and rotational fluid domains. The static fluid domain (blue and grey colour in Fig. 5) represented the region of the cover, inlet and outlet duct, while the rotational fluid domain (red colour in Fig. 5) represented the region near to the rotor.

A complete domain of the non drive end was modelled due to the non-symmetrical design of the inlet and outlet positions. The final CFD model included the stator wall, the rotor assembly, the outlet extrusion and the inlet duct with dual mass flow sensors (Fig. 5). The contact interface between the Solid-Fluid regions and the Fluid-Fluid regions was created by imprinting the mating face to allow conformal mesh between the regions.

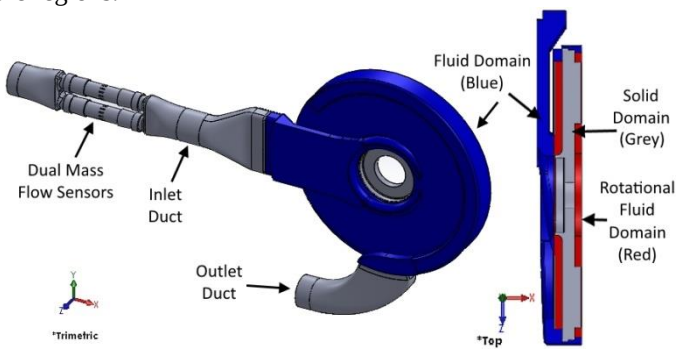

Fig. 5. CFD model including fluid domain (blue), rotational fluid domain (red), rotor & ducting (grey)

Using the automated mesh generation in STAR-CCM+, an unstructured volume mesh (polyhedral cells) was used to discretise the solid and fluid domain. The prism layer was set based on the calculated dimensionless wall distance [24] of (1)-(2) with a local Reynolds number of 3.73*e*5 (3).

$$y^+ = \frac{y u_\tau}{\nu} \quad ; \quad u_\tau \approx \sqrt{\frac{\bar{\tau}_w}{\rho}} \tag{1}$$

where y^+ is the dimensionless wall distance, y is the first cell distance to the wall, u_τ is the friction velocity near to the wall, ν is the kinematic viscosity of air, ρ is the air density and the wall shear stress τ_w is related to the skin friction, C_f in relation to u, the velocity component as follows:

$$\overline{C}_f = \frac{\overline{\tau}_w}{\rho u^2/2} \tag{2}$$

The local Reynolds number is calculated by the rotor angular speed ω, the rotor outer radius R and kinematic viscosity of air ν at 26.85°C of ambient temperature.

$$\mathrm{Re}_\theta = \frac{\omega \cdot R^2}{\nu} \tag{3}$$

A low y+ approach was used to resolve the near wall fluid region, specifically at the tight clearance area of the magnet-to-stator and the rotor-to-cover with a target y+ ≈ 1.

The average mesh count of 13million cells was produced for each one of the three fan blade designs. Fig. 6 presents the computational mesh of fluid domains for the backward-inclined aerofoil blade. A conformal mesh can be seen between the rotational and the static fluid domain. A prism layer of 1.5mm total thickness was created at all surrounding walls in order to solve the boundary layer. Due to the computational power limitation, the cell size for the tight gap between the magnet-stator and the trigger disc-cover could not be improved further. A grid independence study was conducted and the current mesh setup selection was sufficient without losing integrity of the results.

Both fluid domains were set as a single physical model of the air. The air was assumed to have a constant density. This assumption was compared to the equation of state for an ideal gas and the results showed insignificant difference but solved in a longer simulation time compared to when constant density is selected. To draw air naturally by the fan rotation, the inlet was set as a stagnation inlet with 26.85°C air temperature. Other boundary conditions such as the pressure outlet, the static wall on the external walls and the rotational wall on the rotor walls are given in Table I. The heat input was applied at the rotor as a static temperature of 80°C.This was equivalent to the maximum allowable rotor temperature set by the machine manufacturer at full load operation.

A Moving Reference Frame (MRF) approach was applied to the rotational region to mimic the rotational implicitly. This approach allowed the prediction of the rotational flow in the steady state condition and a faster solution compared to a transient simulation [25]. The rotational speed for validation was varied, similarly to the experiment with a backward-inclined aerofoil blade attached.

Three selections of turbulence models, namely SST (shear-stress transport) k-omega [26], Realizable k-epsilon [27] and v2-f model [28]–[31] were compared during the validation. Additionally, SST k-omega with transition model (Gamma ReTheta) [32]–[34] was added in the validation process to find out if there is a potential improvement in the prediction. Table II below shows all the coefficients corresponding to the turbulence models selected. Further, the SST k-omega turbulence model was then chosen for the comparison of the three fan blade designs.

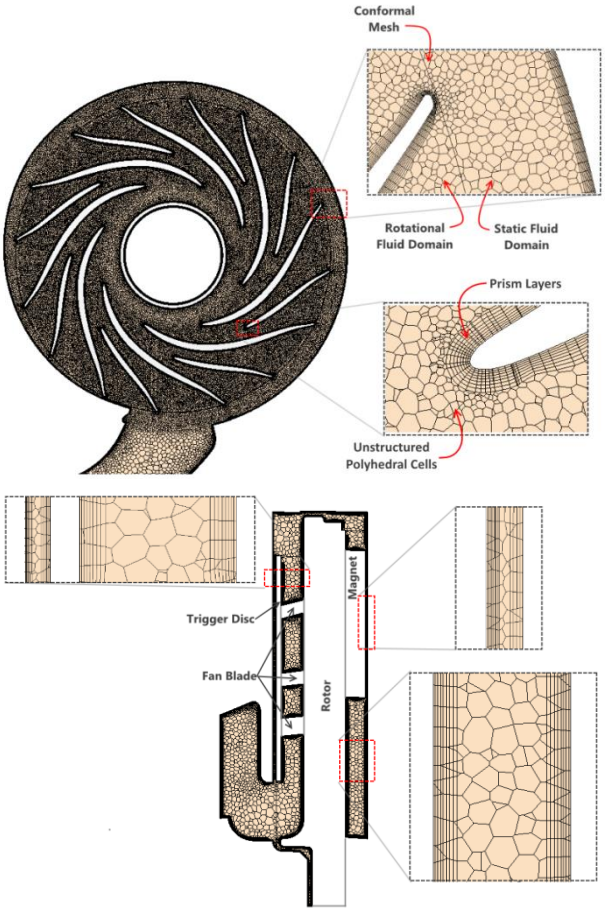

Fig. 6. Computational mesh of fluid domains for backward-inclined aerofoil blade at front cross section (top) and side cross section (bottom).

TABLE I
BOUNDARY CONDITIONS USED FOR ALL SIMULATIONS

Boundary	Conditions
Inlet	Stagnation inlet, p_{total} = 0 Pa, T = 300 K
Outlet	p_{static} = 0 Pa
Stator Wall	Adiabatic no-slip condition wall
Rotor Walls	No-slip condition rotating wall, T = 353.15 K
Cover Wall	Adiabatic no-slip condition wall
Inlet and Outlet Duct	Adiabatic no-slip condition wall

TABLE II
LIST OF COEFFICIENT FOR ALL SELECTED TURBULENCE MODELS

SST		Realizable k-epsilon	
Coefficient	Setup	Coefficient	Setup
Realizability Option	Durbin Scale Limiter	Two-Layer Type	Shear Driver (Wolfstein)
Convection	2nd order	Convection	2nd order
κ	0.41	C_μ	0.09
β^*	0.09	$C_{\epsilon 1}$	1.44
β_1	0.075	$C_{\epsilon 2}$	1.9
σ_{k1}	0.85	C_T	1
$\sigma_{\omega 1}$	0.5	σ_k	1
β_2	0.0828	σ_ϵ	1.2
Realizability Coefficient	0.6	Two-Layer ReY*	60

σ_{k2}	1	Two-Layer Delta ReY	10
$\sigma_{\omega 2}$	0.856		
a_1	0.31		
χ^*	1.5		

V2f		Gamma ReTheta	
Coefficient	Setup	Coefficient	Setup
Realizability Option	Durbin Scale Limiter	Convection	2nd order
Convection	2nd order	σ_f	1
C_μ	0.09	C_{a2}	0.06
$C_{\epsilon 1}$	1.4	C_{e2}	50
$C_{\epsilon 1}$	1.9	σ_{Re_θ}	2
C_τ	6	C_{a1}	2
σ_k	1	C_{e1}	1
σ_e	1.3	C_{θ_t}	0.03
a	0.045	S_1	2
C_1	1.4	Re_{θ_T}	20
$C_{\epsilon 2}$	0.3		
C_L	0.23		
$C_{\mu_{v^2}}$	0.22		
C_η	70		

VI. Experimental Results and CFD Validation

The complete assembly of this machine also has a mesh-filter at the outlet to restrain any contaminant from entering the system. As a result, this filter also restrains the flow and creates an additional pressure drop. In this study, the mesh filter was also included during the experiment to evaluate its restrictiveness.

Fig. 7 shows a comparison of CFD results over measured mass flow rates for the 'with' and the 'without' mesh-filter cases on the outlet. All turbulence models are under-predicting the experimental measurements with insignificant differences between them. However, the CFD models manage to produce a result that shows the same trend over the measurements although the CFD modelling did not include the mesh-filter or any porous region to simulate the pressure drop produced by the filter.

Similar results were obtained by SST k-omega and Realizable k-epsilon, while the v2-f model prediction was close to the measurement with mesh-filter on the outlet. Interestingly, SST k-omega with Gamma ReTheta was not able to produce better results above 2000rpm. Perhaps this is due to the initial assumption of the wall distance term (1.5mm based on the maximum prism layer thickness) for free-stream edges definition. Further investigation is required in order to fully utilise this transition model capability, such as the calibration performed by Malan et al. [36].

It can be observed that the percentage error of all the turbulence models reduced at higher rotational speeds as the flow changed to fully developed turbulent flow. Table III presents an equivalent speed of this machine for transitional flow regime based on the work of Gregory et al. for a generic rotor-stator study [35]. The pattern of mass flow given by CFD started to change after 2500rpm, because of the flow change from transitional to fully developed turbulent flow.

TABLE III
Flow regime given by Gregory et al. [35] with its equivalent speed

Flow regime	Re	Equivalent speed
Transitional flow	1.8e5 < Re < 2.1e5	1690rpm < n < 1970rpm
Fully developed turbulent flow	Re >3e5	n >2810rpm

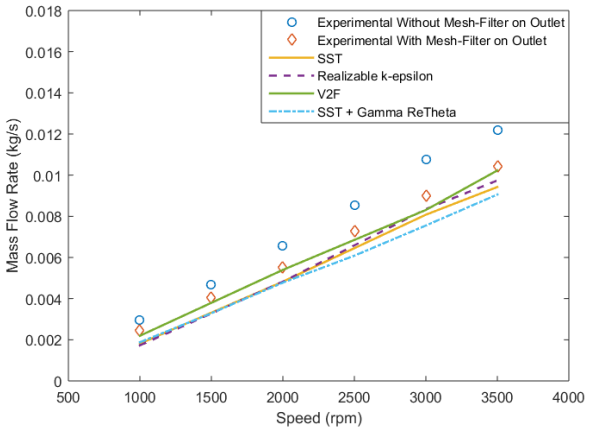

Fig. 7. Comparison CFD and experimental result of (circle) flow without mesh-filter on the outlet, (diamond) with mesh-filter on the outlet.

VII. Results and Discussion

The SST k-omega turbulence model was chosen to assess the different performance of all fan blade designs. This decision was made due to the insignificant difference of the turbulence model results as shown by the CFD validation (Fig. 7). Although the v2-f model is the closest to the experimental data, the model took a longer time to solve because of the nonlinear relationship used to express the eddy viscosity.

A. *Flow Characteristic*

The flow characteristic is important for rotor cooling because it shows how much air can be driven into the system to cool the rotor. This can be evaluated by extracting the mass flow rate of each blade design generated. Additionally, pressure development is needed to estimate the capability of suction or blowing if external ducting is required such as inlet ducting, outlet ducting or filters.

The mass flow rate and pressure rise for the three fan blades are presented in Fig. 8. The radial blade design provides the highest mass flow and pressure development compared to the other designs. The mass flow rate (Fig. 8-a) steadily increases, while the pressure development (Fig. 8-b) sharply rises as the rotational speed increases. On the other hand, the pillar type and the backward-inclined results show similar characteristics for driving the mass flow and pressure development with the same relative difference across the speed range.

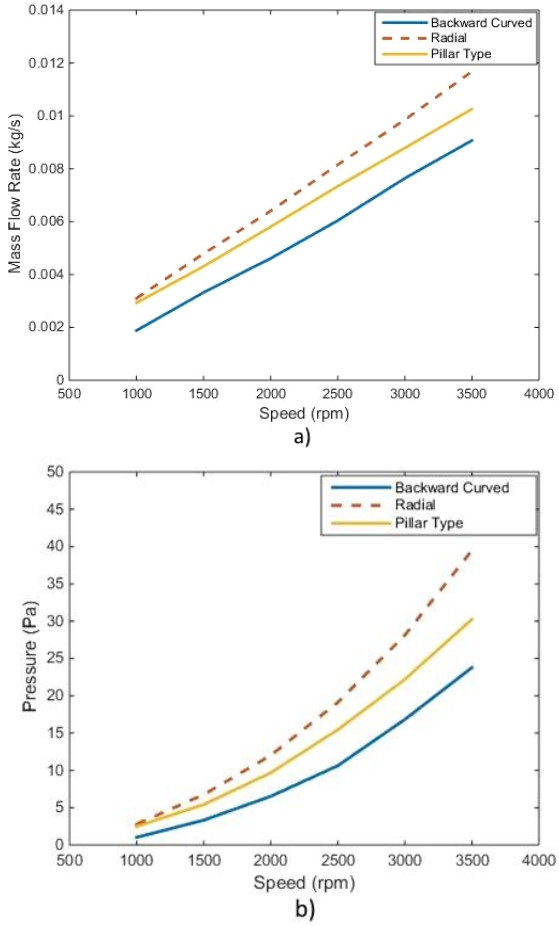

Fig. 8. a) Mass flow rate and b) pressure development of each fan design.

B. *Windage Losses*

In electrical machines, the fan power requirement to spin the rotor at constant speed is equal to the windage losses. This means that the net windage losses are sum of the power requirement due to the fan trying to develop a pressure and the rotor assembly shearing the air. In Fig. 9 it can be observed that the pillar type required the highest power from the machine to spin and gives the highest windage losses, followed by the radial and the backward-inclined design.

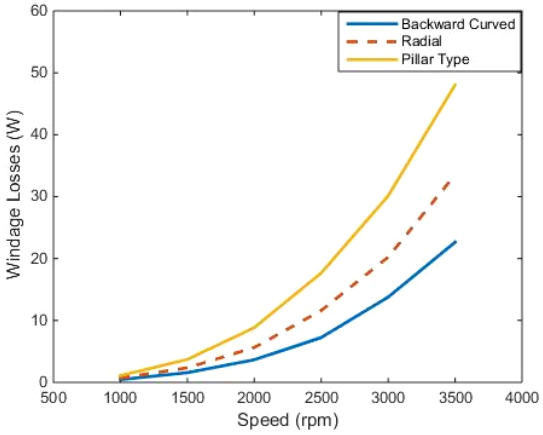

Fig. 9. Windage losses of each fan design.

To further analyse this characteristic, the pressure development of Fig. 8-b and the windage losses of Fig. 9 were normalised to the mass flow rate (Fig. 8-a). Thus, Fig. 10 was introduced in order to compare the fan performance for each individual fan blade design.

In Fig. 10-a, the backward-inclined type provides a fair amount of pressure development across the production of mass flow rate with reasonable amount of windage losses. The fan curve of the radial blade in Fig. 10-b increases sharply and is closely followed by its power curve or windage losses. However in Fig. 10-c, although the pillar type blade design is able to provide a higher amount of mass flow compared to the backward-inclined, this rotor design provides a significant amount of windage loss that increase drastically with increasing mass flow rate.

C. *Thermal Characteristic*

The contour plot of air temperature, Fig.11, was recorded at Z +3mm above the front heated rotor surface for 3500rpm with the range between 26.85˚C to 80˚C. In Fig. 11-a, a hot air patch at 80˚C can be observed on the backward-inclined lower aerofoil surface near to its trailing edge. This hot air then flows to the radial space of the machine while slightly reducing its temperature before going to the outlet. The average air temperature at the outlet of the backward-inclined blade in

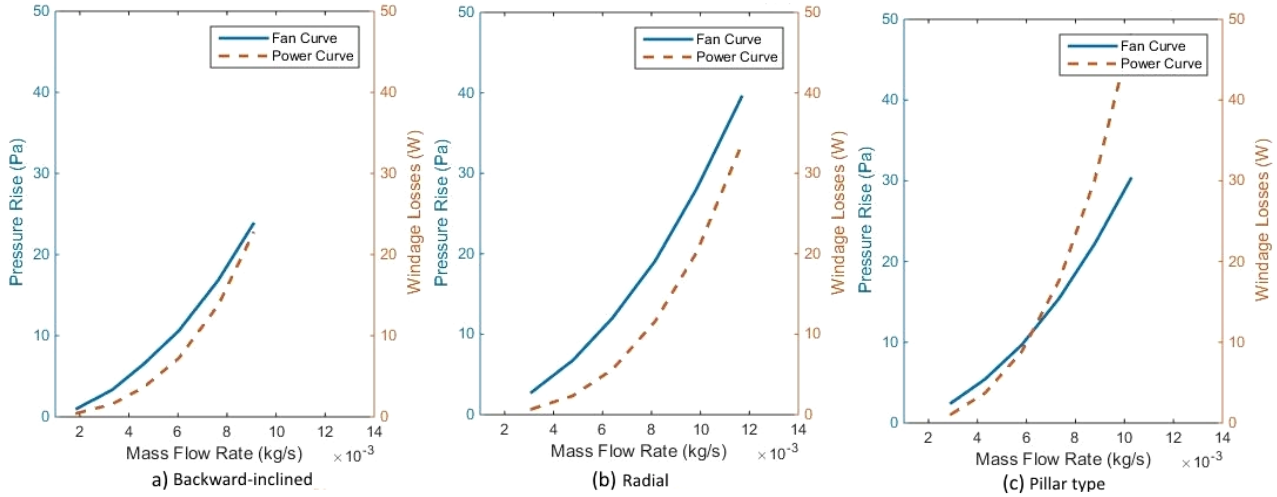

Fig. 10. Fan curve and power curve of (a) backward-inclined aerofoil blade, (b) radial aerofoil blade and (c) tear drop pillar blade.

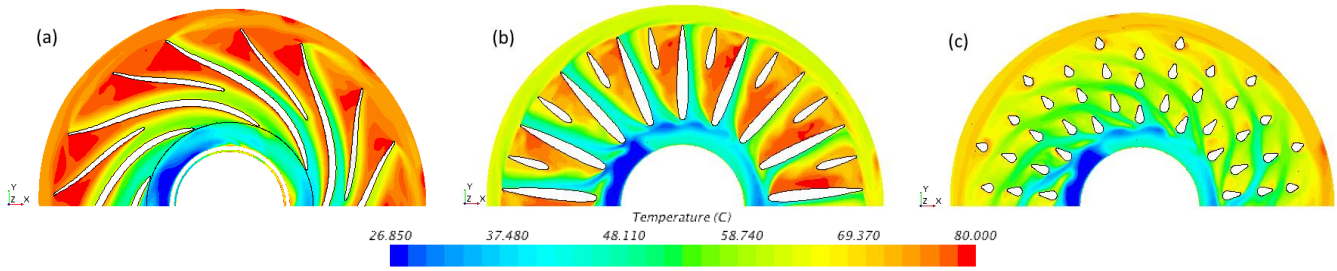

Fig. 11. Air temperature contour at z +3mm from the front heated rotor surface of (a) backward-inclined airfoil blade, (b) radial airfoil blade and (c) tear drop pillar blade.

Fig. 12 displays the highest outlet temperature compared to the other design across the speed range.

Similarly, the radial blade design has multiple hot spots but is smaller compared to the backward-inclined blade design as shown in Fig. 11-b. However, the hot air stays at the downwind region instead of flowing towards the machine radial space. This stagnation hot spot is present because there is flow circulation at the downwind of the radial blades. As a result, the average air outlet temperature of the radial blade design (Fig. 12) was the lowest in drawing the temperature out. It is also observed that the radial blade design almost reaches its thermal steady state at 1500rpm.

On the other hand, no hot spot is present on the air temperature contour plot of the pillar type (Fig. 11-c). Nevertheless it shows a fair temperature gradient that collects at the radial space of the machine compared to the radial blade design. The average air outlet temperature of pillar type (Fig. 12) is marked between the two others fan blade designs with increasing value as the speed increases.

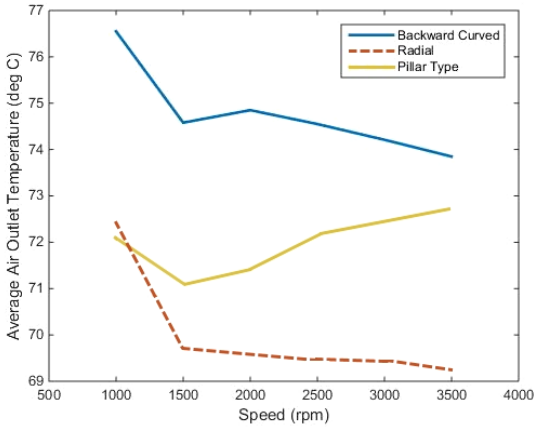

Fig. 12. Average air outlet temperature of each fan design.

Furthermore, the capability of each fan design in dissipating the rotor temperature can be analysed by plotting the average air temperature within the rotating region, as presented in Fig. 13. The hot air patch of the backward-inclined and the radial blade (Fig. 11) proves that both designs have high average temperatures within the system. However, for the radial blade, this hot air remains within the system as discussed before due to the flow circulation at the downwind region of the blade which made the average air outlet temperature (Fig. 12) of this design the lowest.

Based on these factors, the thermal characteristic of each fan design can be evaluated by examining the average heat transfer coefficient. The average heat transfer coefficient in Fig. 14 is calculated by (4) where the heat flux of the rotor and magnet walls are divided by the temperature difference between the rotor and the system average temperature of Fig. 13.

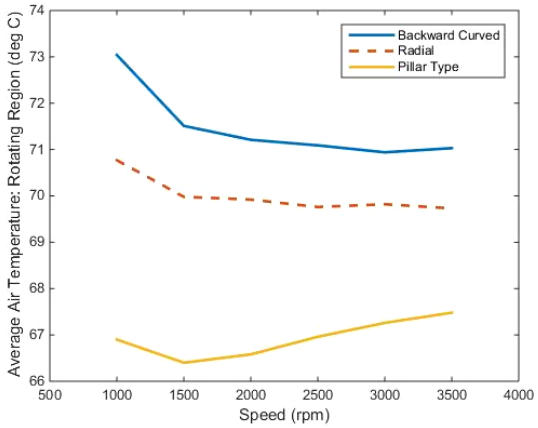

Fig. 13. Average air temperature within the rotating region.

$$h_c = \frac{q''}{\Delta T} = \frac{\dot{m} \cdot C_p \cdot \left(T_{Outlet} - T_{Inlet}\right)}{A \cdot \left(T_{Rotor} - T_{System}\right)} \quad (4)$$

Where h_c is the heat transfer coefficient, q'' is the heat flux, ΔT is the temperature different, $\dot{m}$ is the mass flow rate, C_p is the specific heat capacity of air and A is the rotor heated area.

Fig. 14 shows that the backward-inclined blade design provides high average heat transfer coefficient that almost matches with the radial blade. Although this design provide the lowest mass flow rate, it has the most capability in dissipating the rotor temperature Conversely, better production of mass flow rate of radial blade provides high heat transfer coefficient even with the lowest average air temperature flow through the outlet. Finally, the pillar type has the lowest quantity of the heat transfer coefficient, because it has average mass flow rate and the least value of average air temperature within the system.

The results presented in this section can be used in the LP thermal model, specifically the heat transfer coefficients for the individual components and the windage losses of the rotating parts in the system. This will increase the accuracy of the LP thermal model because these values correspond to the geometrical characteristic that is not included when solving the 1D or 2D analytical model. Optionally, a designer can also input the average heat transfer coefficient versus speed as an equation as given in Table IV.

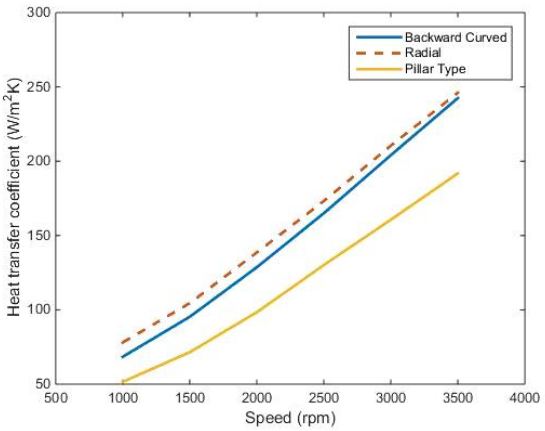

Fig. 14. Average heat transfer coefficient of each fan design.

TABLE IV
BOUNDARY CONDITIONS USED FOR ALL SIMULATIONS

Blade Design	Regression
Backward-Inclined	$y = -3E\text{-}09x^3 + 2E\text{-}05x^2 + 0.0074x + 39.894$
Radial	$y = -3E\text{-}09x^3 + 2E\text{-}05x^2 + 0.0079x + 48.643$
Pillar Type	$y = -4E\text{-}09x^3 + 3E\text{-}05x^2 - 0.0164x + 41.821$

D. *Rotor Cooling Performance Index (RCPI)*

The authors would like to propose an index to differentiate the performance of each fan blade design for AFPM rotor cooling application. The Rotor Cooling Performance Index (RCPI) will benefit when comparative analysis of fan blade design is required. The assessment can be done by experimental or CFD analysis and provides the data needed to calculate the convective heat transfer, q, and the windage losses, W. These two values then are divided to produce the RCPI number as shown in equation (5).

$$RCPI = \frac{Convective\,HT}{Windage\,Losses} = \frac{q}{W} \tag{5}$$

The value produced is dimensionless because both parameters' units are in Watt. A user can implement this index either for a specific intended rotational speed or across a broad range of speeds. For example, at 2000rpm, the RCPI of the backward-inclined blade is 61.03 compared to 49.02 for the radial blade and 29.47 for the pillar type. These values indicate that at 2000rpm, the backward-inclined blade outperforms the radial blade and the pillar type by a factor of 1.25 and 2.07 respectively. In other terms, the higher the RCPI number, the better cooling capability that a fan design produces.

In this study, the RCPI of all selected blade designs can be plotted across a range of speed as shown in Fig. 15. All blade designs show that higher cooling performance was achieved at lower speed and the performance declines when the rotational speed increases. This happens because at higher rotational speed, the windage losses start to dominate (Fig. 9) and at the same time the capability of the air to absorb the heat from the system (Fig. 13) is stabilised.

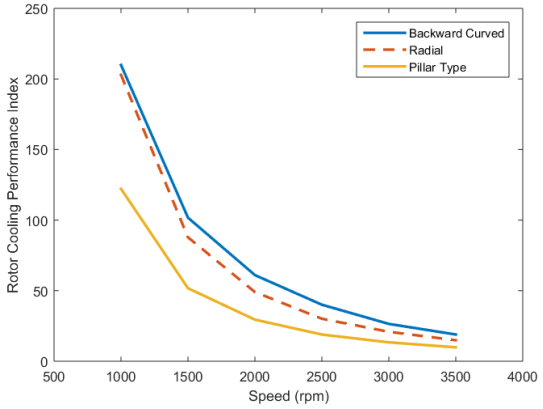

Fig. 15. Rotor Cooling Performance Index (RCPI) curves for this study.

VIII. CONCLUSION

A comparative study of different fan blade designs for rotor cooling of axial flux permanent magnet machines by CFD has been presented. Firstly, the mass flow rate from CFD and experimental measurements with the three turbulence models selected were validated. It was found that the CFD modelling of the mass flow rate was under-predicted and insignificantly different given by all the three tested turbulence models. Further validation on the thermal analysis is required in order to conclude regarding the capability of CFD modelling for predicting the heat transfer for this specific study.

The study of the characteristics of three fan blade designs has shown that each design has its own merit. Firstly, the backward-inclined design gives a fair amount of flow characteristics and windage losses. The radial design offers the highest flow characteristics with a cost of high windage losses. Finally, the pillar type needs high power requirements to provide good flow characteristics. The simulation results with the same static rotor temperature have been presented to investigate the thermal characteristics of these fan blade designs.

Additionally, the Rotor Cooling Performance Index (RCPI) is introduced to assess the cooling performance of each fan blade design. This is done by dividing the cooling capability over the power requirement to spin the rotor. Here, although the backward-inclined provides the best performance, this design is limited for an unidirectional application.

Both flow and thermal characteristics studied in this paper could be an input to a lumped parameter thermal model in order to achieve accurate thermal predictions for AFPM machines.

In the future, this study will be extended by using fixed loss densities to simulate the temperature distribution in solid domains. Further study is also required to investigate the full capability of rotor cooling techniques for a AFPM machine.

IX. ACKNOWLEDGMENT

The authors would like to thank YASA Motor Ltd., Dr. Humberto Medina, Mr. Chris McCaw and Mr. David Mackenzie for their support and assistance.

X. REFERENCES

[1] *Directive 2009/28/EC of the European Parliament and of the Council 23 April 2009*, Official Journal of the European Union, L 140/16 – L 140/62, 2009. [Online]. Available: http://eur-lex.europa.eu/legal-content/EN/TXT/?uri=CELEX:32009L0028

[2] *Commission Regulation (EC) No 640/2009 of 22 July 2009*, Official Journal of the European Union, L 191/26 – L 191/34, 2009. [Online]. Available: http://eur-lex.europa.eu/legal-content/EN/TXT/?uri=CELEX%3A32009R0640

[3] J. Gieras, M. Kamper and R. Wang, *Axial Flux Permanent Magnet Brushless Machines*. 2nd ed. Dordrecht: Springer Science + Business Media B.V, 2008, pp. 1-10.

[4] H. Vansompel, "Design of an Energy Efficient Axial Flux Permanent Magnet Machine", Ph.D. dissertation, Ghent University, Belgium, 2013.

[5] E. Odvářka, A. Mebarki, D. Gerada, N. Brown and C. Ondrůšek, "Electric Motor-Generator for a Hybrid Electric Vehicle", *Engineering Mechanics*, vol. 16, no. 2, pp. 131-139, 2009.

[6] T. Woolmer and M. McCulloch, "Analysis of the Yokeless And Segmented Armature Machine", *2007 IEEE International Electric Machines & Drives Conference*, pp. 704 - 708, 2007.

[7] A. Fitzgerald, C. Kingsley Jr and S. Umans, *Electric machinery*. New York: McGraw-Hill, 2003. Sixth edition. pp 668-674

[8] D. Kothari and I. Nagrath, *Electric machines*, 4th ed. New Delhi: Tata McGraw-Hill Education, 2010, pp. 250-258.

[9] K. N. Gyftakis, M. Sumislawska, D. Kavanagh, D. Howey and M. McCulloch, "Dielectric Characteristics of Electric Vehicle Traction Motor Winding Insulation under Thermal Ageing", *IEEE Transactions on Industry Applications*, early access.

[10] M. Sumislawska, K. Gyftakis, D. Kavanagh, M. McCulloch, K. Burnham and D. Howey, "The Impact of Thermal Degradation on Properties of Electrical Machine Winding Insulation Material", *IEEE Transactions on Industry Applications*, accepted 2016.

[11] D. Howey, A. Holmes and K. Pullen, "Prediction and measurement of heat transfer in air-cooled disc-type electrical machines", *5th IET International Conference on Power Electronics, Machines and Drives (PEMD 2010)*, pp. 1-6, 2010.

[12] R. Wang, M. Kamper and R. Dobson, "Development of a Thermofluid Model for Axial Field Permanent-Magnet Machines", *IEEE Transactions on Energy Conversion*, vol. 20, no. 1, pp. 80-87, 2005.

[13] C. Lim, J. Bumby, R. Dominy, G. Ingram, K. Mahkamov, N. Brown, A. Mebarki and M. Shanel, "2-D lumped-parameter thermal modelling of axial flux permanent magnet generators", *Electrical Machines, 2008. ICEM 2008. 18th International Conference* on, pp. 1-6, 2008.

[14] Y. Chong, D. Magahy, J. Chick, M. Mueller, D. Staton and A. McDonald, "Numerical modelling of an axial flux permanent magnet machine for convection heat transfer", *IET Conference on Renewable Power Generation (RPG 2011)*, pp. 1-6, 2011.

[15] G. Airoldi, G. Ingram, K. Mahkamov, J. Bumby, R. Dominy, N. Brown, A. Mebarki and M. Shanel, "Computations on heat transfer in axial flux permanent magnet machines", *2008 18th International Conference on Electrical Machines*, pp.1-6, 2008.

[16] A. Boglietti, A. Cavagnino, D. Staton, M. Shanel, M. Mueller and C. Mejuto, "Evolution and Modern Approaches for Thermal Analysis of Electrical Machines", *IEEE Transactions on Industrial Electronics*, vol. 56, no. 3, pp. 871-882, 2009.

[17] A. Fawzal, R. Cirstea, K. Gyftakis, T. Woolmer, M. Dickison and M. Blundell, "The fan design impact on the rotor cooling of axial flux permanent magnet machines", *2016 XXII International Conference on Electrical Machines (ICEM)*, pp. 2725-2731, Lausanne, Switzerland, Sept. 2016.

[18] R. Camilleri, T. Woolmer, A. Court and M. McCulloch, "Investigation into the temperature profile of a liquid cooled YASA© AFPM machine", *6th IET International Conference on Power Electronics, Machines and Drives (PEMD 2012)*, pp. 1-8, 2012.

[19] R. Camilleri, D. Howey and M. McCulloch, "Predicting the Temperature and Flow Distribution in a Direct Oil-Cooled Electrical Machine With Segmented Stator", *IEEE Trans. Ind. Electron.*, vol. 63, no. 1, pp. 82-91, 2016.

[20] *P400 Series: Compact axial flux motors and generators*, Abingdon: YASA Motors Ltd., 2016. [Online]. Available: http://www.yasamotors.com/wp-content/uploads/2015/09/YASA_P400_Product_Sheet.pdf

[21] *YASA-400: Axial flux electric motor*, Abingdon: YASA Motors Ltd., 2016. [Online]. Available: http://www.yasamotors.com/wp-content/uploads/2015/09/YASA-400-Product-Sheet.pdf

[22] H. Bloch and C. Soares, *Process plant machinery*. Boston: Butterworth-Heinemann, 1998, pp. 520-525.

[23] L. Wallis, E. Leonardi, B. Milton and P. Joseph, "Air Flow and Heat Transfer in Ventilated Disc Brake Rotors with Diamond and Tear-Drop Pillars", *Numerical Heat Transfer, Part A: Applications*, vol. 41, no. 6-7, pp. 643-655, 2002.

[24] H. Schlichting and K. Gersten, *Boundary-layer theory*, 8th ed. Berlin: Springer, 2000, pp. 517-522,

[25] M. Darvish and S. Frank, "Toward the CFD Simulation of Sirocco Fans: From Selecting a Turbulence Model up to the Role of the Cell Shapes", in *FAN2012: International Conference on Fan Noise, Technology and Numerical Methods*, Senlis, France, 2016, pp. 1-12.

[26] F. Menter, "Two-equation eddy-viscosity turbulence models for engineering applications", *AIAA Journal*, vol. 32, no. 8, pp. 1598-1605, 1994.

[27] T. Shih, W. Liou, A. Shabbir, Z. Yang and J. Zhu, "A New K-epsilon Eddy Viscosity Model for High Reynolds Number Turbulent Flows: Model Development and Validation", *Ntrs.nasa.gov*, 1994. [Online]. Available: http://ntrs.nasa.gov/search.jsp?R=19950005029.

[28] P. Durbin, "Separated flow computations with the k-epsilon-v-squared model", *AIAA Journal*, vol. 33, no. 4, pp. 659-664, 1995.

[29] P. Durbin, "On the k-3 stagnation point anomaly", *International Journal of Heat and Fluid Flow*, vol. 17, no. 1, pp. 89-90, 1996.

[30] F. Lien, G. Kalitzin and P. Durbin, "RANS modeling for compressible and transitional flows", in *Center for Turbulence Research - Proceedings of the Summer Program*, pp. 267-286, 1998.

[31] L. Davidson, P. Nielsen and A. Sveningsson, "Modifications of the V2 Model for Computing the Flow in a 3D Wall Jet", *Proceedings of the International Symposium on Turbulence, Heat and Mass Transfer, October 12 - 17, 2003, Antalya, Turkey*., vol. 4, pp. 577-584, 2003.

[32] R. B. Langtry, "A Correlation-Based Transition Model Using Local Variables for Unstructured Parallelized CFD Codes," Doctoral Thesis, University of Stuttgart, 2006.

[33] F. R. Menter, R. B. Langtry, S. R. Likki, Y. B. Suzen, P. G. Huang, and S. Volker, "A Correlation-Based Transition Model Using Local Variables Part 1 --- Model Formulation," *Proc. ASME Turbo Expo*, June 14-17, Vienna, Austria, 2004.

[34] R. B. Langtry, K. Sengupta, D. T. Yeh, A. J. Dorgan, "Extending the Local $\gamma - Re_{\theta_T}$ Correlation based Transition Model for Crossflow Effects," *AIAA Fluid Dynamics Conference 2015*, June 22-26, Dallas, TX, USA., 2015.

[35] N. Gregory, J. Stuart and W. Walker, "On the Stability of Three-Dimensional Boundary Layers with Application to the Flow Due to a Rotating Disk", *Philosophical Transactions of the Royal Society A: Mathematical, Physical and Engineering Sciences*, vol. 248, no. 943, pp. 155-199, 1955.

[36] Malan P., Suluksna K ., Juntasaro E.,"Calibrating the gamma- ReTheta Transition Model for Commercial CFD", *47th AIAA Aerospace Sciences Meeting*, Jan 2009.

XI. BIOGRAPHIES

Ahmad Syahid Fawzal was born in Selangor, Malaysia on November 1982. He received the Diploma of Engineering Technology in Machine Building and Maintenance from Universiti Kuala Lumpur Malaysia France Institute (UniKL MFI) (2007), continued for a BEng in Mechanical Engineering at University of Derby, UK (2009) and MSc in Computational Fluid Dynamics at Cranfield University, UK (2012).

His employment between of his study included CFD consultancy for oil & gas industry at BMT Fluid Mechanics Ltd. and machine reliability consultant (vibration) at AF Condition Monitoring (M) Sdn Bhd. He is currently a Ph.D candidate at Coventry University. His research interests include windage losses, fan performance, thermal and cooling of electrical machines.

Remus M. Cirstea was born in Brasov, Romania, on February 1979. He holds a degree in Automotive Engineering from Transilvania University, Brasov, Romania (2002) and a Master's degree in Automotive Engineering from Coventry University, UK (2009).

He then worked as a research assistant with Coventry University as part of the Low Carbon Technology Project (2010-2012) and after that he increased his commitments towards teaching undergraduate and postgraduate students. He is currently Course Director for the MSc Automotive Engineering programme at Coventry University and a lecturer in fluid dynamics. His

research activities involve external aerodynamics for vehicle with focus towards the cooling drag on vehicles due to momentum loss in the airflow.

Konstantinos N. Gyftakis (M'11) was born in Patras, Greece, on May 1984. He received the Diploma in Electrical and Computer Engineering from the University of Patras, Patras, Greece in 2010.

He pursued a Ph.D in the same institution in the area of electrical machines condition monitoring and fault diagnosis (2010-2014). Then he worked as a Post-Doctoral Research Assistant in the Dept. of Engineering Science, University of Oxford, UK (2014-2015).

He is currently a Lecturer, School of Computing, Electronics and Mathematics, Faculty of Engineering, Environment and Computing and an associate with the Research Centre for Mobility and Transport, Coventry University, UK. His research activities are in fault diagnosis, condition monitoring and degradation of electrical machines. He has authored/co-authored more than 40 papers in international scientific journals and conferences.

Tim J. Woolmer was born in Oxford 1981. He holds an Engineering degree and a DPhil from Oxford University.

In 2009 he founded YASA Motors Ltd., and now works there as the CTO. He has published a number of papers and patents on the YASA motor and related technologies. His research interests include magnetic, thermal and mechanical design

Mike Dickison was born in Farnborough, Hampshire in 1959. After completing an MSc in Automotive Product Engineering at Cranfield, he had a 23 year career working in automotive consultancies.

After initially working in the structural analysis and test fields, he subsequently led complete vehicle engineering programmes with responsibility for both technical and commercial aspects. For the past 7 years Mike has been working at Coventry University, where he is an Associate Dean in the Faculty of Engineering, Environment & Computing. Mike's research interests include lightweight structures and low carbon vehicle technologies.

Mike Blundell is well known for his work in vehicle dynamics and the use of multi-body systems (MBS) software. Prior to joining the University he worked for the ship and submarine design department of the Ministry of Defence and for Boeing (Europe). During the 1980s he was an early user of ADAMS working for Tedas Ltd the original distributers of the ADAMS software in Europe. After joining Coventry University in 1991 he led their research in the vehicle dynamics area with a particular focus on tyre modelling and the efficient use of MBS software.

Major projects have included a collaborative EPSRC/Airbus project looking into aircraft tyre modelling and a European 6th Framework project considering occupant safety in Helicopter crashes. Recent and current work has involved the Niche Vehicle Project, the Low Carbon Vehicle Technology Project and European funded work modelling the protection of civil infrastructures from terrorist attacks.